Tellus
SERIES B
CHEMICAL
AND PHYSICAL
METEOROLOGY
PUBLISHED BY THE INTERNATIONAL METEOROLOGICAL INSTITUTE IN STOCKHOLM

Tellus (2010), 62B, 316–328

Differences between trends in atmospheric CO_2 and the reported trends in anthropogenic CO_2 emissions

By R. J. FRANCEY*, C. M. TRUDINGER, M. VAN DER SCHOOT, P. B. KRUMMEL, L. P. STEELE and R. L. LANGENFELDS, *Centre for Australian Weather and Climate Research/CSIRO Marine and Atmospheric Research, Aspendale, Vic. 3195, Australia*

(Manuscript received 19 November 2009; in final form 24 June 2010)

ABSTRACT

Averaged annual accumulation of CO_2 in the atmosphere, dC_a/dt, has been slowing from peak growth in 2002/2003 associated with anomalous climate-induced emissions at high northern latitudes. This slowing is widespread but determined with greatest certainty in the largest well-mixed portion of the global troposphere (30°S–90°S). We rely on atmospheric mixing for global integration and selection of atmospheric data for spatial representativeness. Prior to 2002/2003, after empirical adjustment for perturbations associated with ENSO and volcanic activity (EV), dC_a/dt increases are well represented by linear regression, using direct monitoring records from 1990 or 1965, also from pre-industrial times using archived air. In contrast, modelled atmospheric trends due to reported emissions dC_E/dt (assuming historically consistent oceanic and terrestrial uptake mechanisms), agree with dC_a/dt or dC_a/dt-EV up until 1990, are near-stable through the 1990s and increase by 29% between 2000 and 2008. Using atmospheric constraints based on trends in both dC_a/dt-EV and interhemispheric gradient, the differences between trends in dC_E/dt and atmospheric CO_2 growth are most simply explained as an artefact of underestimating 1994–2003 emissions by around 6%. This is achieved with a near constant post-1965 airborne fraction; otherwise unusually complicated sink changes are required for the period.

1. Introduction

Canadell et al. (2007) conclude that 2000–2006 economic activity, carbon intensity and efficiency of natural sinks contribute to accelerating atmospheric CO_2 growth. Expanded detail is provided by Raupach et al. (2007, 2008). They include an estimate of ocean uptake by Le Quéré et al. (2007), who report reduced effectiveness of the Southern Ocean CO_2 sink due to climate change. These studies use emission estimates of fossil fuel burning and cement-production by Marland et al. (2008), and land-use change (LUC) by Houghton (2008), based largely on national emissions reported to the United Nations Framework Convention on Climate Change (UNFCCC). Recent increasing emissions are attributed primarily to Asia (Gregg et al., 2008). More recently, Le Quéré et al. (2009) highlight a 29% increase in reported emissions since 2000 and conclude that reduced uncertainty in natural sinks is required to improve definition of the global carbon cycle. A decreasing trend in natural sinks is supported by modelled global changes in ocean uptake (Sarmiento et al., 2009) and, for example, by changes in South Indian Ocean fugacity measurements relative to that in the atmosphere (Metzl, 2009). In the Le Quéré and Sarmiento inversion studies, atmospheric CO_2 growth is derived from concentrations reported to international databases, with little discussion of potential measurement or sampling bias.

Our focus has been minimization of uncertainty in global trends in atmospheric CO_2 growth (dC_a/dt), which, irrespective of contributing processes, relate most directly to changes in climate forcing.

After a general discussion of measurement and sampling bias in Section 2, Section 3 demonstrates an overall slowing in dC_a/dt since 2002/2003 in a record from Cape Grim (Tasmania, 41°S) employing in situ CO_2 monitoring with unprecedented temporal precision and, more significantly, rigorous selection of hourly data that results in unusually large spatial representativeness.

The growth trend is assessed against historic data introduced in Section 4, which includes four-decade trends in Scripps Institution of Oceanography records (Keeling et al. 2001, 2005; http://scrippsco2.ucsd.edu/data/data.html) from Mauna Loa (MLO Hawaii, 21°N) and/or South Pole (SPO, 90°S). We also use the trend in interhemispheric gradient in mixing ratio (MLO-SPO). On subdecadal timeframes, the four-decade Scripps records are used to provide an empirical description relating interannual variations in dC_a/dt with climate and volcanic

*Corresponding author.
e-mail: roger.francey@csiro.au
DOI: 10.1111/j.1600-0889.2010.00472.x

activity, permitting assessment of their likely contribution to the most recent Cape Grim dC_a/dt trends. Section 4 concludes with an estimate of the atmospheric trends (dC_E/dt) anticipated from reported emissions, which are obtained using a simple box model that closely describes the carbon budget on decadal timescales since pre-industrial times.

Section 5 extends the analysis of CSIRO CO_2 measurements over two decades and provides additional constraints on the location of emissions and sinks by way of relative trends at different latitudes, using data from a global flask sampling network (these are more representative of data submitted to global databases, for example, http://gaw.kishou.go.jp/wdcgg/; http://www.esrl.noaa.gov/. . ./globalview). The flask dC_a/dt data are processed in a similar manner to that used in Section 3, and growth rate uncertainties compared. The box model is used to estimate the magnitude of source and sink changes that are required to reconcile the differences in the recent dC_a/dt and dC_E/dt trends.

The analyses are discussed in Section 6 and conclusions summarized in Section 7.

2. Sampling and selection issues

2.1. Site selection

Optimal sampling strategies to obtain global CO_2 growth rate changes are different from those that seek information on regional carbon budgets. Averaging data from many sites, to address sampling and measurement uncertainties (WMO, 2008; http://www.esrl.noaa.gov/gmd/ccgg/trends/index.html#global), incorporates sampling bias and can obscure fine detail in high-quality records. This is a critical issue for Northern Hemisphere (NH) boundary-layer sampling sites that are embedded in an atmospheric mixing volume overlaying 70% of the global land mass, associated with the bulk of industrial emissions and also includes major rapidly exchanging, climate-sensitive plant carbon reservoirs. Even with common hemispheric climate forcing and relatively rapid within-hemisphere mixing (of order 3 weeks), large spatial (horizontal and vertical) and temporal heterogeneity in NH CO_2 exists.

Denning et al. (2004) report that interhemispheric CO_2 mixing times for 12 atmospheric transport models range from 0.5 to 1.3 yr for 3-D models (longer for 1-D and 2-D models). The main barrier to N–S mixing is at the southern edge of the intertropical convergence zone (Miyazaki et al., 2008). Since the time for interhemispheric mixing (is much greater than that for within-hemisphere mixing, air sampled south of 30°S provides an effective integration of the heterogeneous northern fluxes, limiting the possibility of overrepresentation of regional northern fluxes in a global total. Then, selection of mid-to-high latitude southern air to minimize recent land contact can lead to significant advantages in representing global growth rate changes.

This argument depends on the very small spatial gradients and interannual variability in those gradients at mid-to-high southern latitudes; for example, typical background CO_2 fields >30°S have annual horizontal gradients <0.2 ppm, vertical gradients <0.1 ppm km^{-1}, well-characterized seasonal amplitude ~0.5 ppm. Aircraft vertical CO_2-profiling summarized by Stephens et al. (2007), presents mid-day profiles from 12 global locations. The Cape Grim (41°S) data, representing 10 yr of monthly flights in clean air conditions, show the smallest gradients, seasonally and vertically, and are given emphasis below. Of the NH sites, the Hawaiian site Mauna Loa best exhibits these properties and is treated independently in this study as a way of indicating sensitivity to hemisphere differences.

2.2. Measurement error

There are several potential growth rate errors in CO_2 time series that are not well addressed in international data repositories or metadata. They are examined in detail in Appendix S2, establishing that resulting bias in the CSIRO records used here is small, and more generally, errors are less likely to be a significant influence after the 1980s. Thus, averaging data from many sites to overcome measurement error is unjustified, particularly when larger uncertainty due to sampling bias can be introduced by the averaging process.

2.3. Data selection

Selecting data from individual site records to reconstruct global trends requires attention to potential bias in measured growth rate, and to sampling strategies that minimize local or regional contamination. Cape Grim provides unusual opportunities to assess both issues by having several CSIRO operated CO_2 monitoring programs with different measurement, calibration and sampling strategies. For example, they include an on-going automated comparison of measurements on the same flask-air that closely compares CSIRO and National Oceanic and Atmospheric Administration USA, Earth System Research Laboratory (NOAA ESRL) measurements at this site (Masarie et al., 2001); differences in smoothed data from CSIRO and NOAA programs remain within ~0.05 ppm.

We select 'baseline' CO_2 hours that require moderate to high wind speeds (>5 m s^{-1}) from the marine wind-direction sector that meet a CO_2 stability criterion of <0.3 ppm in the hourly mixing ratios over five successive hours. For these hours, hourly radon measurements (a signal imposed by air passage over land, decaying with 3.8-d half life) confirm a marine boundary layer origin. For example, from 2001 to 2007, 36% of hours with wind speeds >2 m s^{-1} have a median concentration of 37 mBq m^{-3} (Zahorowski et al., 2005; W. Zahorowski, personal communication 2009), compared to a 100 mBq m^{-3} we have historically used as a baseline threshold. Appendix S1 shows typical 10-d back trajectories for conditions when Cape Grim radon is

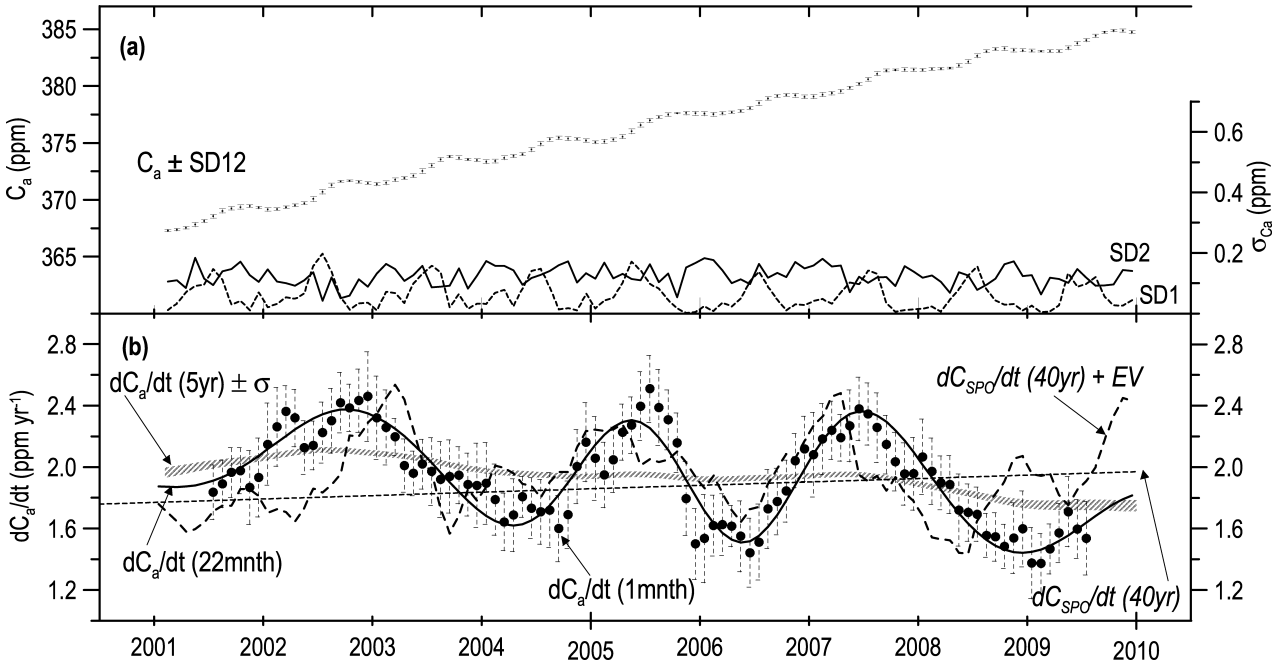

Fig. 1. (a) The left axis quantifies the increasing monthly average CO_2 mixing ratio with uncertainty (vertical error bars, SD12 = $(SD1^2 + SD2^2)^{1/2}$) measured in Cape Grim air with a high-precision in situ LoFlo analyser, and selected for maximum spatial representation (see text). The right hand axis shows SD1, standard deviation in the monthly values of an 80-d smoothing spline, and SD2, standard deviation in residuals of hourly values from the spline ($n \sim 200$). (b): CO_2 growth calculated from (a) data using three different time resolutions (1 month, filled symbols with vertical error bars; 22 months shown as a smooth black line; 5 yr, using shading to represent uncertainty limits; see text). These are compared to a four-decade linear trend (short dashes) measured at SPO, and trend plus variability (long dashes) driven by Niño3.4 monthly data.

<100 mBq m^{-3}; recent land contact (not counting Antarctica) is excluded on >99% of occasions. Thus the composition of Cape Grim baseline air frequently closely resembles that in the free troposphere.

3. Growth rates from the Cape Grim LoFlo in situ monitoring

Since 2001, CO_2 has been monitored at Cape Grim, a location with frequent exposure to Southern Ocean marine boundary layer air, with unprecedented temporal stability, and with advanced infrastructure that enables selection and verification of the origin of the air. Of records examined, this provides recent multiyear trends in atmospheric CO_2 growth with the smallest uncertainty, and is used here to introduce methods to quantify the uncertainty.

The LoFlo analyser (Da Costa and Steele, 1999; Francey and Steele, 2003) demonstrates in monthly measurements of air in seven attached high pressure cylinders, each with mixing ratios assigned on the WMO Mole Fraction scale by the WMO Central CO_2 Calibration Laboratory; between 2001 and 2010 the standard deviation of monthly determinations of near-ambient cylinder air relative to the other six, and in more-transient ambient 'reference' gases relative to the seven-cylinder scale, is typically ±0.003 ppm. The analyser samples 190 ± 77 baseline hours per month (with a seasonal range of 135 ± 58 in April, 19% of hours, to 253 ± 44 in December, 34% of hours).

Figure 1a shows the mean monthly mixing ratio, and its uncertainty SD12 calculated by combining the standard deviation (SD1) of daily values subtracted from a smoothing spline through the selected hourly data with 50% attenuation at 80 d (mainly representing bias from incomplete sampling of the seasonal cycle throughout the month), and the standard deviation (SD2) of the residuals of each selected hourly value about the smoothing spline for that month. Since 2001, the mean *LoFlo* monthly SD12 = $(SD1^2+SD2^2)^{1/2}$ is 0.15 ± 0.03 ppm.

Figure 1b derives growth rates, dC_a/dt, from the monthly mixing ratios using three different methods for calculating dC_a/dt. The smooth solid line represents the widely used time-differential of a 22-month smoothed trend curve through deseasonalized data (Thoning et al., 1989). High time resolution (1 mnth) growth rates are obtained by annual differencing of values for corresponding months, plotted at the mean time, and combining uncertainty SD12 of the individual months (using the square root of the sum of squares). The 5-yr smoothed growth trends (5 yr), shown as a ±<u> shaded band, are obtained from the first derivative of a spline fit to the monthly mixing ratio data with 50% attenuation at 5 yr while propagating the SD12 monthly uncertainties through the splines (Enting et al., 2006).

There is a high degree of consistency between the three methods of determining dC_a/dt. The 5-yr trend deceases from a peak of 2.11 ± 0.02 ppm yr^{-1} in 2002.6, through 1.84 ± 0.02 ppm yr^{-1} in 2008.5, to 1.79 ± 0.04 ppm yr^{-1} in 2010.0. This is unexpected at a time when reported emissions from 2000 to 2008.5 have increased by 29%. Figure 1b also shows that the LoFlo trend is slowing relative to, and falling significantly below, the four-decade trend at SPO over this period (dashed linear regression, denoted '40 yr'). That this is unlikely to be the result of climate variation is implied by the reasonable agreement in the amplitude and phasing of interannual variability driven primarily by ENSO data (dashed curve). These dashed 'baselines' are derived in the next section (and used above with an initial assumption that monthly data can be scaled using empirical coefficients derived from 9-month smoothed dC_a/dt, and ENSO and volcanic indices).

4. Historic growth rate behaviour

Figure 2a shows the 22-month smoothed dC_a/dt (Thoning *et al.*, 1989) over five decades from MLO and SPO, where the large time span reduces the significance of measurement and sampling bias on mean behaviour. Data shown in Fig. 2 contribute to the following background information used in this study:

4.1. Linear dC_a/dt trends

Figure 2a provides linear regressions through data from 1965 to 2006; the SPO regression is that used in Fig. 1b. Data prior to 1965 are not used due to significant data gaps in the SPO record (which may contribute to the unusual early interannual behaviour in the SPO dC_a/dt), and to the occurrence at the start of the record of explosive volcanic activity (Mt. Agung, 1963) that may unduly bias the regressions (in the sense of making the difference from the Fig. 1b LoFlo trend even greater). The fact that the MLO increase is marginally faster than that at SPO is consistent with increasing emissions that are mainly located in the NH.

4.2. Interhemispheric gradient

Figure 2b shows the difference ($C_{MLO} - C_{SPO}$) obtained from the 22-month smoothing spline through monthly mixing ratio data. It is well represented by the linear regression and is also attributed to increasing emissions that are mainly located in the NH. In Section 5.1, we use this relationship between dC_a/dt and ($C_{MLO} - C_{SPO}$) to constrain the location of sources and/or sinks that might reconcile reported emission and measured atmospheric trends.

4.3. Interannual variability

The dC_a/dt variation attributable to ENSO and volcanoes (EV) used in Fig. 1b is empirically estimated from the CO_2 monthly data used in Fig. 2a, using an independently developed approach similar to that of Raupach et al. (2008).

Compared to the Raupach et al. (2008) approach, our analyses are restricted to data from 1965, after which we place significance in the fact that the amplitude of interannual variation at SPO is consistently equal to or less than that at MLO. Also, the ENSO and volcano time-series are extended, and weighted separately for positive (+) and negative (−) climate anomalies to accommodate the suggestion (Reichstein et al., 2009) that 'the response of the ecosystem carbon balance to climate variability

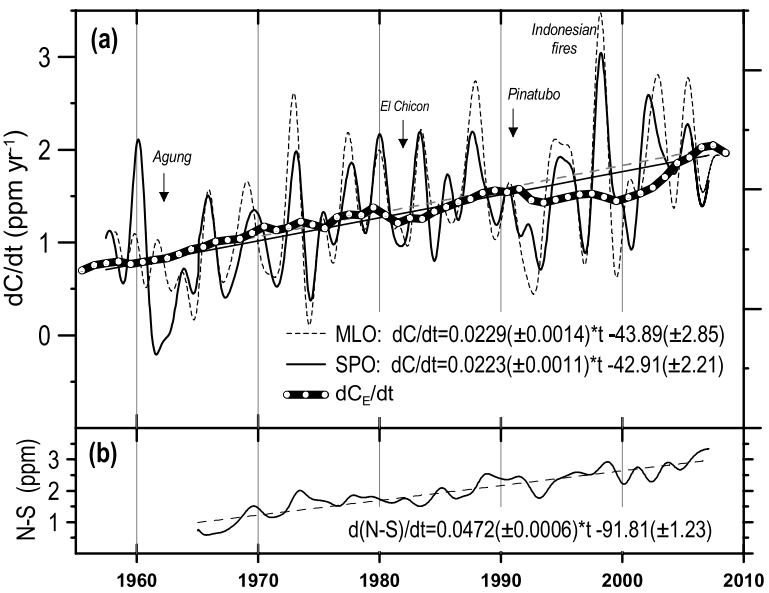

Fig. 2. (a) Long-term growth rates (ppm yr^{-1}) from Mauna Loa (MLO, 20°N) and South Pole (SPO, 90°S) measured by Scripps Institution of Oceanography. Growth rates are obtained by differentiation of the smoothed trend curve through monthly mixing ratios (Thoning et al., 1989). Linear regressions are fitted to the 1965–2006 data of each trend curve (and extrapolated to provide a baseline). Anomalous events thought to influence CO_2 growth are indicated. The thick line with overlaid white symbols shows an estimate of changes due to reported anthropogenic emissions (Section 4.4). (b) The interhemispheric gradient obtained by subtracting the SPO mixing ratio trend from that at MLO, also fitted with a linear regression.

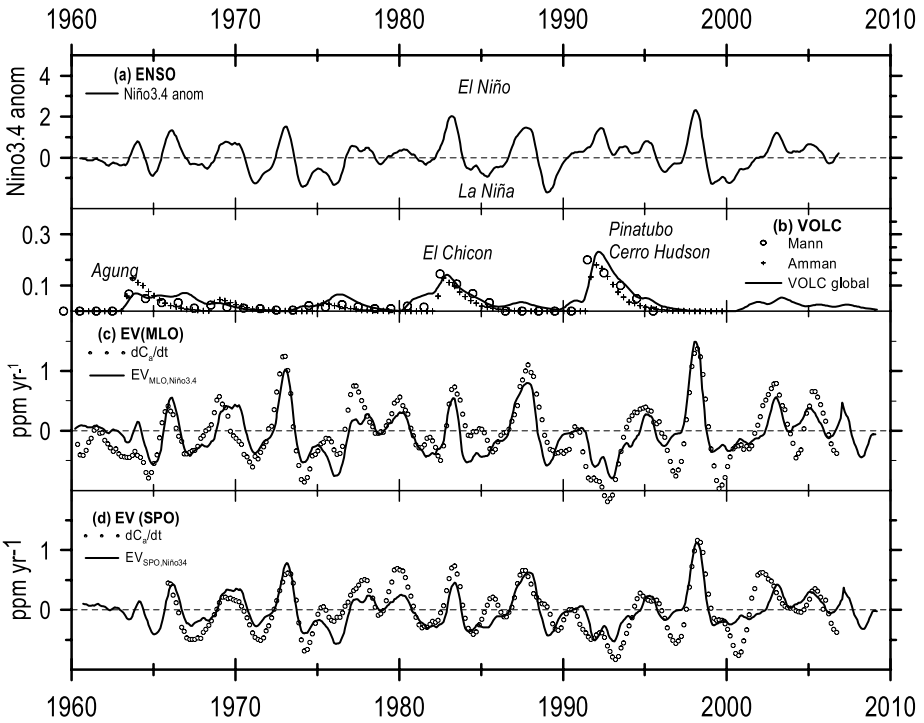

Fig. 3. Niño3.4 anomalies, smoothed with 9-month running means, used for the empirical derivation of EV using eq. (1). Volcanic indices, smoothed with 9-month running means, for the empirical derivation of EV using eq. (1). (c) EV_{MLO} (line) compared to detrended MLO dC_a/dt (symbols). (d) EV_{SPO} (line) compared to detrended SPO dC_a/dt (symbols).

is highly skewed, i.e. large carbon losses are much more likely than large carbon gains during periods with climatic conditions deviating from normal'. Thus,

$$\mathrm{EV} = a_0 + a_1\mathrm{ENSO}^{+}(t - t_{\mathrm{lag}}) + a_2\mathrm{ENSO}^{-}(t - t_{\mathrm{lag}}) + a_3\mathrm{VOLC}(t), \quad (1)$$

where EV is obtained using least squares fitting of MLO or SPO growth rate anomalies, ENSO is a climate anomaly index that precedes a CO_2 growth variation by t_{lag} months (t_{lag} ranges between 3 and 12 months); VOLC describes the influence of major volcanic eruptions. Using 1965–2006 MLO and SPO data with Fig. 2 regressions subtracted, we solve for a_i and t_{lag} using different ENSO and VOLC anomalies (selected examples shown in Figs 3a, 3b. Appendix S3 provides correlation (r) and lag details for a range of ENSO and volcanic indices, and smoothing parameters of 5, 9 and 22 months. For all indices, the EV are derived separately for MLO and SPO dC_a/dt.

Selecting the 9-month smoothing on all parameters, Figs 3c and d compare EV ($r = 0.8$, $t_{\mathrm{lag}} = 4$ months) with the MLO, SPO dC_a/dt anomalies. Only results for Niño3.4 (sea-surface temperature anomalies generated to highlight climate sensitivity) are presented here for discussion. The EV explain up to 60% of the interannual variability in dC_a/dt, and are insensitive to site or smoothing. The positive anomalies are marginally more strongly correlated; all tested indices provide similar overall conclusions, as discussed in Appendix S3.

Examination of Fig. 3 suggests that unexplained CO_2 growth-rate variation is mainly systematic rather than randomly distributed noise, and results from variations in the magnitude of responses to ENSO and volcanoes. Since, on average, the EV reflect CO_2 fluxes from equatorial vegetation (Rayner et al., 2008), it is likely that the proximity of individual equatorial flux events to particular measurement sites, or non-equatorial events, contribute much of the unexplained variance. If the processes that lead to CO_2 perturbations varies between ENSO events this may also contribute to variance.

With this perspective we consider separate interannual events in the context of available independent evidence for unusual flux processes or anomalous climate forcing. Information about these events can define the sense, if not the magnitude of anomalous contributions, and need to be considered when presenting statistically based conclusions. For example, differences in forcing processes are indicated for recent interannual events in 1992–1994, 1997–1998, 1999–2002 and 2002–2003:

- The 1992–1994 perturbation is widely attributed to volcanic activity (e.g. Jones and Cox, 2001).
- The 1997–1998 departures are associated with record ENSO emissions from the equatorial Indonesian wild fires

involving unusual contribution from burning of recently exposed peat (Langenfelds et al., 2002; Page et al., 2002). It will be seen below that this signal is similarly expressed in northern and southern latitudes.

- The 1999–2002 dip is yet to be specifically addressed in the literature, though it does coincide with the major anomaly since 1982 in the $\delta^{13}CO_2$ versus CO_2 record (Allison and Francey, 2007). The timing also corresponds to unique anomalies in ocean records over the period (Ashok et al., 2007; Dore et al., 2009), also a quiet period in ENSO related wild fires (Randerson et al., 2005, 2009). This is the subject of a separate study.
- The 2002–2003 anomaly has been associated with drought in America and Europe (emissions of ∼0.2–0.3 PgC; Vetter et al., 2008), and significant wild fire activity in Siberia (emissions of ∼0.5 PgC; Rayner et al., 2008). It will be seen below that this event is expressed quite differently at northern and southern latitudes.
- We also note in passing, that interhemispheric difference anomalies in both CO_2 and $\delta^{13}CO_2$ suggest unusual northern terrestrial emissions in 2006.

As a further example, correlations summarized in Appendix S3 explore the influence of record length using post-1965 CO_2 data, and post-1980 data only; for SPO data there is no difference, but MLO based correlations are stronger using post-1980 data, which we attribute to the regional proximity of MLO to the major equatorial events in the 1990s (probably aided by the mean location of the ITCZ being north of the equator).

4.4. Historic growth changes attributable to emissions

Figure 2a also includes a model estimate of the atmospheric growth trend that can be attributed to reported emissions. Trudinger et al. (1999) demonstrate close agreement over the last century between trends in reported emissions and smoothed CO_2 growth (in contemporary post-1960 air plus Antarctic ice-core and bridging firn and archived air samples), using simple parametrizations of ocean and terrestrial sinks (see Appendix S4). Here we use updated estimates of emissions due to fossil fuel burning (from G. Marland) and land use change (from R. Houghton) used by Le Quéré et al. (2009). The modelled atmospheric growth changes attributable to these emissions, dC_E/dt, while not including natural interannual variability, provide a convenient baseline for examining recent observed dC_a/dt trends. Our modelled change in global sinks is an increase by ∼0.9 PgC yr^{-1} per decade (with partitioning not tightly determined but approximately equally distributed between land and oceans).

5. Measured atmospheric growth from global flask sampling

To get a global and two-decade perspective on the Fig. 1 Cape Grim LoFlo measurements discussed in Section 3, we use data from the CSIRO global atmospheric sampling network (Francey et al., 1996). However, it is instructive to first examine the relative trends between flask sites and flask measurement laboratories, using a simple method of comparing annual average mixing ratios to remove seasonal influence, and using differences from South Pole annual averages to suppress interannual variation that is similarly expressed in both hemispheres.

5.1. Relative trends

In Fig. 4 we present CO_2 data from the CSIRO global flask network for which consistent two-decade measurements exist. Italicized lower case site labels are used for CSIRO flask records to distinguish them from Scripps MLO and SPO sites and measurement methodology, and include sampling from Alert (*alc*,

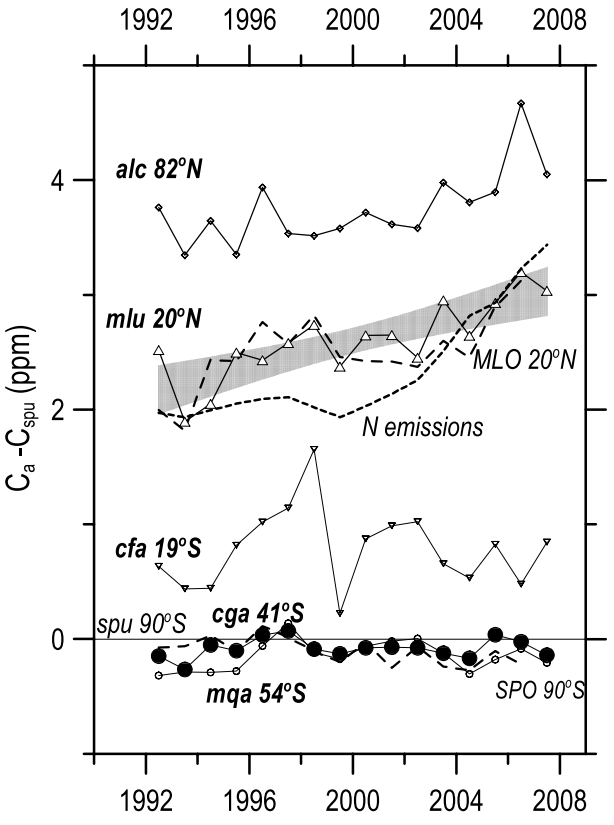

Fig. 4. Temporal dependence of CO_2 meridional differences: Annual average values of monthly CSIRO CO_2 for Alert (*alc*, 82°N), Mauna Loa (*mlu*, 20°N), Cape Ferguson (*cfa*, 19°S), Cape Grim (*cga*, 41°S) and Macquarie Island (*mqa*, 54°S) expressed as a difference from the South Pole annual mean. A linear regression is shown only for *mlu*, along with 95% confidence intervals (shaded region). Thin medium dashes are for Scripps MLO and SPO data (with CSIRO *spu* subtracted). The thick short dashes for the *mlu* case illustrate the trend expected from dC_E/dt, by applying the relationship between the linear regressions in Figs 2a and b.

82°N), Mauna Loa (*mlu*, 20°N), Cape Ferguson (*cfa*, 19°S), Cape Grim (*cga*, 41°S) and Macquarie Island (*mqa*, 54°S).

The difference between Scripps and CSIRO increases slowly to ∼0.1 ppm over two decades (most clearly seen in the SPO-*spu* record, however the mean difference MLO-*mlu* before 2000 is positive, and after 2000 is negative, the change being of similar sign and magnitude to the change in SPO-*spu*). Possible calibration bias in one or other (or both) of the laboratories is discussed in Appendix 2. The difference is not significant in the present context, particularly when we use only CSIRO data that is precisely linked to a common local scale. Temporal consistency in the differences is well within 0.1 ppm.

The very small measured spatial gradients and small interannual variability at the mid-to-high southern latitudes are consistent with the CO_2 homogeneity in this large globally representative region. The increasing relative trends in the *mlu*, *alc* and MLO records are consistent with NH emissions being primarily responsible for increasing CO_2, with larger interannual variability reflecting the greater NH land/transport influences. A linear regression through the *mlu-spu* data in Fig. 4 gives a similar slope of 0.057 ± 0.011 ppm yr^{-1} compared to the long-term slope in Fig. 2b of 0.047 ± 0.001 ppm yr^{-1}. Interannual variability at *cfa* (on the Great Barrier Reef, 19°S) reflects proximity to land sources and more complex meteorology, and possibly reflects Indonesian peat fires in 1997/98 (Langenfelds et al., 2002; Page et al., 2002); however an overall trend in *cfa* relative to *spu* is not evident.

Note that a significant early 1990s volcanic anomaly is not evident in Fig. 4 despite the well-documented volcanic influence on global growth rate (Jones and Cox, 2001). The absence of a perturbation on the interhemispheric difference is consistent with CO_2 uptake by the equatorial terrestrial biosphere (as a result of environmental changes triggered by the Pinatubo eruption), a perturbation that has been propagated similarly to both hemispheres.

In Fig. 2, the consequence of NH fossil emissions over four-decades is a near-linear 1 ppm yr^{-1} change in dC_a/dt, matched by a near-linear 2 ppm change in C_{MLO}-C_{SPO}, with both trends attributed to increasing anthropogenic emissions in the NH. The post-2000 dC_E/dt increase of 0.7 ppm yr^{-1} over 7 yr is predominantly attributed to NH Asian fossil emissions data (Gregg et al., 2008). In the absence of other explanations for these trends, we estimate (on time frames long compared to interhemispheric mixing) changes in N–S gradient on the basis of its historic relationship with emissions. Based on the relationship between the linear regression slopes in Figs 2a and b the Mauna Loa-South Pole difference expected from dC_E/dt is illustrated by the dashed line superimposed on the *mlu-spu* curve of Fig. 4. The estimated 1990s flattening and ∼1.4 ppm C_{MLO}-C_{SPO} change since 2000 are not observed in the flask interhemispheric gradient, with the biggest difference occurring in the decade starting in 1992. We rather observe a gradual increase since 1992.

5.2. Flask growth rates

We limit dC_a/dt discussion to Mauna Loa (*mlu*) and Cape Grim (*cga*) flasks which, of data that we have detailed information, best represent their respective hemispheres. Figure 5 highlights uncertainties in growth-rates on both monthly and 5-yr smoothed time frames, for comparison with Fig. 1. Consistent with our suggestion that *mlu* is more susceptible to nearby equatorial and within-NH influences, the record exhibits larger scatter, and interannual excursions in the monthly data than *cga,* and a larger uncertainty band in the 5-yr trends. Of particular note is the 2002–2003 period which shows the largest consistent difference between interannual variability in *mlu* dC_a/dt (symbols) and that in the EV index; this is far less evident at Cape Grim.

Here, monthly mixing ratio data are the mean of measurements on two to six flasks (<1 h total sampling in selected clean-air conditions) per month, whereas the LoFlo data of Fig. 1, despite much more rigorous selection criteria, involve 190 ± 77 h per month. Uncertainty combines SD1, the standard deviation of an 80-d smoothed curve through the individual flask data with the standard deviation SD2 of individual flask residuals around the smooth curve. Compared to the LoFlo record, where, in ppm, $SD12 = 0.15 \pm 0.03$; for the flask records $SD12 = 0.18 \pm 0.07$, 0.50 ± 0.22 for *cga*, *mlu*, respectively. The uncertainty for flask data at both sites is multiplied by 3 to recognize the sparse sampling of each month and less rigorous selection (for example, synoptic variability is not captured, and this is more serious at Mauna Loa due to the large seasonal and latitudinal gradients in CO_2 fields, discussed in Section 2.1). The 5-yr spline bands propagate ±3*SD12 uncertainties. However, the respective 5-yr trends agree within spline uncertainties and exhibit a similar pattern; the pattern is similar to that in the LoFlo record from 2001. Relative 5-yr trends (ppm yr^{-1}) in the three records are:

	Cape Grim (*LoFlo*)	Cape Grim *(cga)*	Mauna Loa (*mlu*)
2002.6	2.11 ± 0.02	2.07 ± 0.13	2.20 ± 0.41
2008.5	1.84 ± 0.02	1.85 ± 0.16	1.68 ± 0.53

The close agreement between the Cape Grim *LoFlo* and *cga* trends suggests that the three times SD12 multiplier overestimates uncertainty at this site, and the less stringent selection criteria used for flask sample collection are effective in representing the large scale SH homogeneity. As calculated, the changes in the flask data are of marginal significance, even at *mlu* where the indicated decrease is largest.

5.3. Flask growth rate trends versus emission trends

To aid comparison of measured atmospheric trends to trends in emission estimates, we suppress 'natural' variability in the dC_a/dt by subtracting the empirically derived EV (Section 4.3). Figure 6 includes the changes expected from the emission

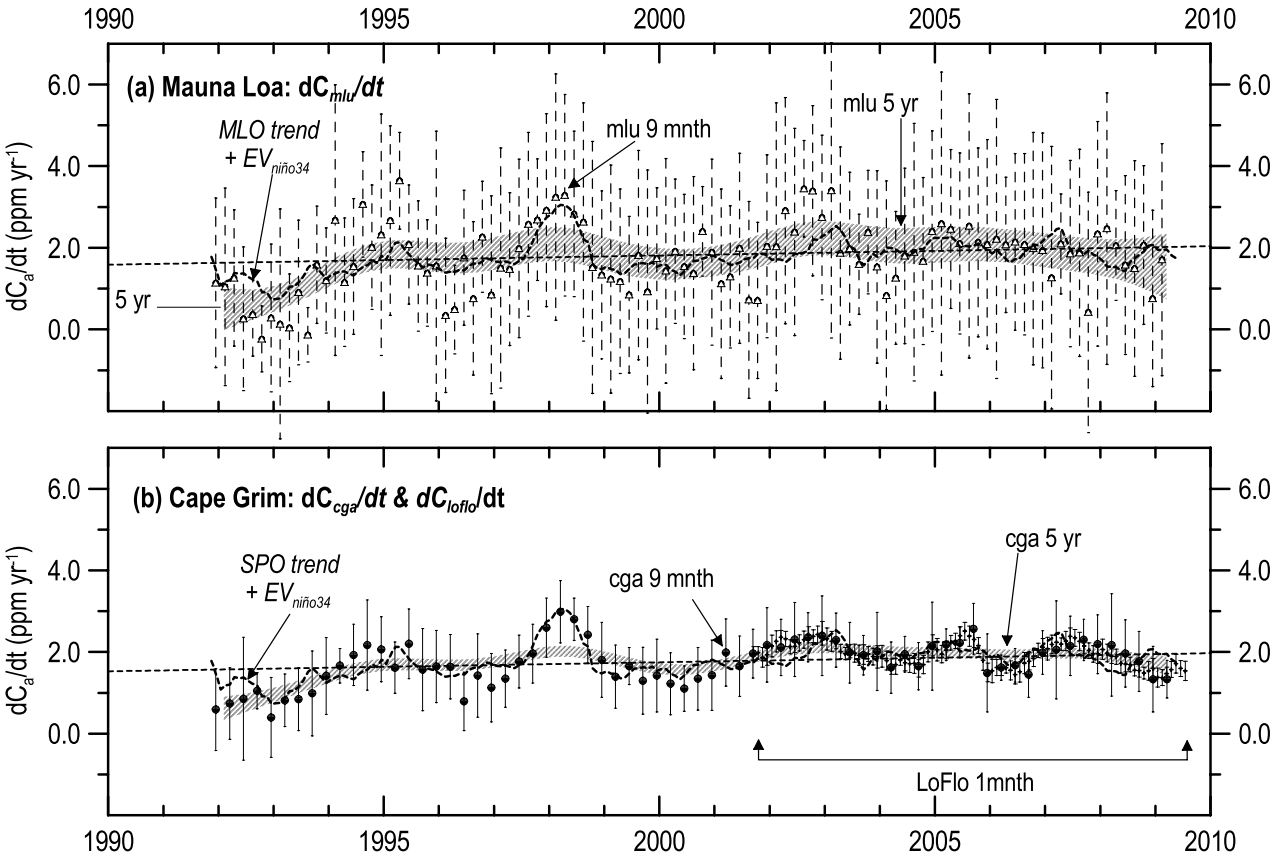

Fig. 5. The growth rate dC_a/dt (ppm yr^{-1}) using monthly values with ±3*SD12 uncertainties obtained from annual differences in the mean monthly mixing ratios; 5-yr smoothed values, shown with shading, represent the mean trend ± uncertainty obtained by differentiation of a smoothing spline (Enting et al., 2006). (a) Uses Mauna Loa (*mlu*) flask air collected and measured by CSIRO (open circles, with error bars plotted every third month). The MLO four-decade linear regression (light dashes), and regression plus $EV_{nino3.4}$ (dark dashes), are included for comparison. (b) Uses Cape Grim (*cga*) flask air collected and measured by CSIRO (filled circles). The SPO four-decade linear regression (light dash), and regression plus $EV_{nino3.4}$ (dark dash), are included for comparison. Panel (b) also includes the selected monthly LoFlo data from Fig. 1b (dots with error bars from 2002).

estimates, dC_E/dt, as a thick line with overlaid white symbols and the four-decade SPO dC_a/dt as a linear, thin, dashed line.

In Fig. 6a, *cga* and *mlu* growth rates with uncertainties are obtained by applying the Enting et al. (2006) method on monthly mixing ratios ±3*SD12 using 9-month smoothing; EV determined using 9-month smoothed monthly values of Niño3.4 anomalies, advanced by 4 months, are subtracted. Uncertainties combine the dC_a/dt spline uncertainties with 0.4*Niño3.4 anomalies. Figure 6 shows (dC_{mlu}/dt-EV) and (dC_{cga}/dt-EV) with unadjusted dC_{cga}/dt for comparison. The *mlu* variability remains significantly greater than that at *cga*. The *cga* cases show that adjustment for the major volcanic event in 1991–1994 is significant, but perhaps incomplete, since this is the most significant departure of (dC_{cga}/dt-EV) data from the four-decade SPO trend.

The 1997–1998 peak is reduced, and adjustment is noticeable around 2003. The small ENSO activity after 2003 is indicated by the small adjustments.

Overall, significant interannual variability persists in these curves (possibly due to reasons outlined in Section 4.3, and suggesting that a more sophisticated treatment of interannual variability may reduce the natural variability even further); however between 1994 and 2003 the dC_E/dt passes through the lowest points in the (dC_{cga}/dt-EV) curve, rising to peak values in 2007. The EV adjustment does not provide an explanation for the dC_a/dt decline quantified in Fig. 1.

This is emphasized in Fig. 6b, with expanded y-scale, which uses 5-yr smoothing of the dC_a/dt-EV values. In this case, the uncertainties fed to the spline fitting are amplified to represent the persisting interannual variability seen in (a), using a minimum monthly uncertainty determined by the standard error in the y-residuals from a linear regression through the dC_a/dt-EV of Fig. 6a. This has the effect of reducing the difference between uncertainty bands from the three records. The dC_E/dt is well below these uncertainties between 1994 and 2003, rising above the uncertainty bands in 2007.

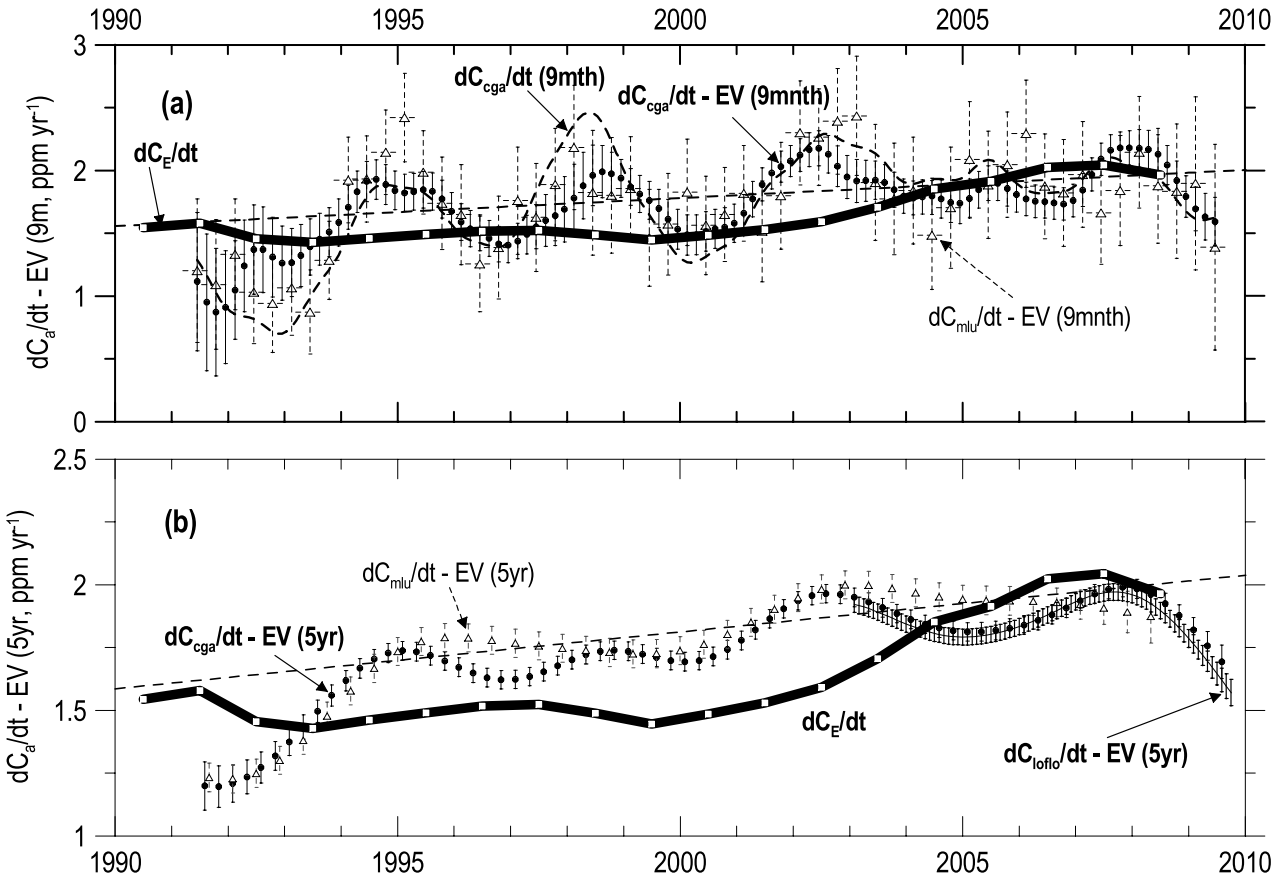

Fig. 6. (a) Monthly values of annual CO_2 growth adjusted to reduce long-term mean interannual variation (dC_a/dt-EV). Vertical uncertainty estimates derived from differentiation of 9-month smoothing of dC_a/dt and EV indices for *cga* (filled circles, plotted every second point) and *mlu* (open triangles, every third point) records; unadjusted dC_{cga}/dt is included (dark dashed line) for comparison. The modelled trend due to emissions, dC_E/dt (thick line with overlaid white symbols) and SPO four-decade linear regression (light dashes) are included in (a) and (b). (b) Five-year smoothed dC_a/dt-EV values for *mlu* (open triangles, plotted every third point), *cga* (filled circles, every second point) and *loflo* (line with error bars, every point).

6. Discussion

From the early 1990s (after the large volcanic perturbation), Fig. 6 shows dC_E/dt systematically below ENSO adjusted atmospheric trends (dC_a/dt-EV) then rapidly rising from 2000 to exceed the atmospheric parameter by 2007. This behaviour is quite closely mirrored in the differences between observed and anticipated interhemispheric trends in Fig. 4 (but starting earlier because of the presumed equatorial location of vegetation that is influenced by Mt. Pinatubo eruption, thus the interhemispheric gradient is not significantly perturbed).

After 2007, slowing emissions lead to a slowing in dC_E/dt, e.g. in Fig. 6b, such that the good agreement before 1990 (see Fig. 2) is again achieved, and the interhemispheric gradient is consistent with this. It is possible that this includes a CO_2 response to the 2007–2009 Global Financial Crisis (Le Quéré et al., 2009). However the situation will be better evaluated with improved time resolution and sensitivity to growth rate calculation away from end-effects, and when the behaviour of the current ENSO cycle is better defined.

6.1. *Fluxes required to reconcile atmosphere and emission trends*

To estimate the magnitude of fluxes (anthropogenic or natural) required resolving the apparent trend conflicts over the last two decades, we can quantify differences between dC_E/dt and dC_a/dt-EV as discrepancies in the source estimates or departures from modelled sink behaviour. Figure 7 reproduces results from Fig. 6, but presenting annual average values in PgC yr^{-1}, taken from 1994.5 to avoid the early-1990s volcanic influence. Figure 7b shows the emissions required to match dC_a/dt -EV in Fig. 7a, assuming ongoing C_a-dependent ocean and terrestrial modelled uptake (each steadily increasing at ∼0.04 PgC yr^{-1} yr^{-1}). For convenience we present adjustments to emissions, but these could also represent the magnitude of global

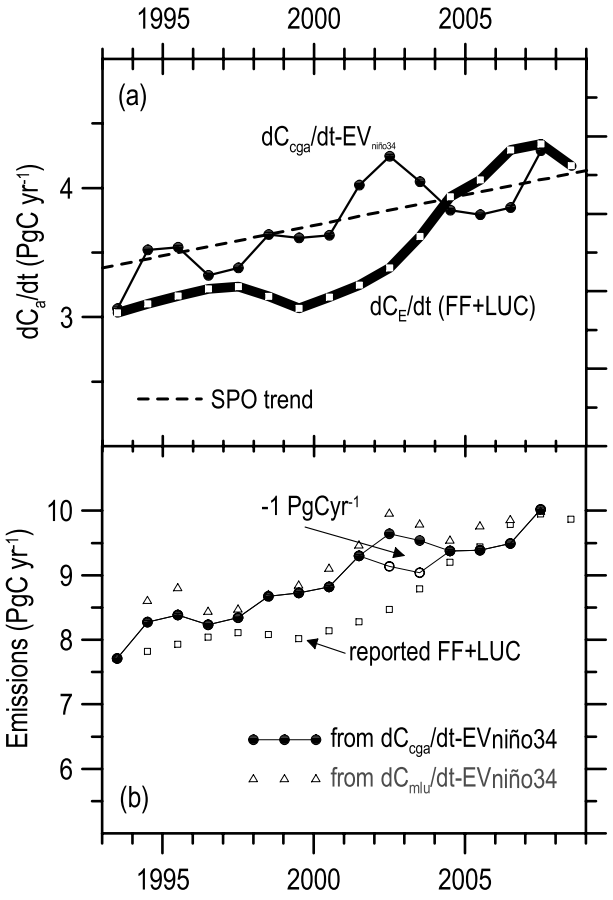

Fig. 7. (a) Shows annual values of measured atmospheric growth adjusted for EV in PgC yr^{-1}. obtained from the *cga* monthly data in Fig. 6a. The modelled dC_E/dt using reported emissions, and the long-term mean SPO trend are included for comparison. (b) Uses the model to calculate emissions PgC yr^{-1} (filled symbols) that are consistent with the atmospheric measurements from *cga*; emissions calculated using *mlu* (open symbols) are also included for comparison. The –1 PgC yr^{-1} adjustment to the *cga* curve addresses high northern latitude emissions in 2002–2003 that are not captured by the predominantly equatorially forced EV index (see text). These exceed the reported emissions (open squares) between 1994 and 2004.

sink anomalies that are required for consistency with reported emissions. The 2002/2003 peak is not well captured in the predominantly equatorially forced empirical EV. The adjusted line with open symbols in Fig. 7b illustrates the result of attributing extra emissions of 1 PgC yr^{-1}, spread over 2002 and 2003 for the dC_{cga}/dt-EV$_{Niño3.4}$ case, reducing the difference from dC_E/dt in this period. After 2003, and in the absence of independently documented sink anomalies, dC_{cga}/dt decreases on average from the peak while reported emissions continue to increase strongly until 2007, before declining to agree with the four-decade SPO trend by 2009.

Between 1994 and 2003, the difference between the reported and modelled emissions (for the adjusted dC_{cga}/dt-EV$_{Niño3.4}$ case) is 5.1 PgC over 10 yr, and, for example, is the largest sustained difference between the dC_E/dt and the MLO, SPO linear trend lines in Fig. 2. If interpreted as an error in emissions, the difference over the 1994–2003 period would represent an underestimation of 7% in the fossil fuel and cement emissions (reported total 67 PgC), or 34% of the reported LUC component (15 PgC), that is about 6% in total anthropogenic emissions. Alternatively, the combined modelled ocean and terrestrial sinks used in estimating dC_E/dt (49 PgC) are 20% overestimated.

Trends in global sink behaviour are often discussed in terms of changes in airborne fraction (the proportion of total anthropogenic emissions that remain in the atmosphere, e.g. Raupach et al., 2008). In determining trends and uncertainties in airborne fraction behaviour, it is important to acknowledge the possible sampling and emission biases discussed in this paper. Assuming that the measures adopted above effectively remove bias, the model airborne fraction using adjusted annual emissions to fit the dC_{cga}/dt-EV$_{Niño3.4}$ is near-constant after 1965 at 0.42 $\pm$ 0.02% (and for example, is 0.41 $\pm$ 0.02% after 1990).

6.2. *Decadal sink changes*

If the relatively stable estimates of emissions through the 1990s is correct, and is due to slowing of NH emissions, then our suggested combined atmospheric constraints of global growth trends and interhemispheric gradient trend require a northern non-fossil source of carbon ($\sim$20% above the historic values given by the Trudinger et al. (1999) model for the period) to maintain the interhemispheric gradient.

For the period of acceleration in the post-2000 reported emissions, a rapidly increasing northern sink might explain the absence of change in the interhemispheric gradient, but would not provide sufficient net CO_2 to explain the recent observed annual growth rates. An effective source (reduced sink) in the Southern Hemisphere (SH) that balances interhemispheric gradient, would lead to recent atmospheric growth rates significantly above those observed, unless there is a coordinated equatorial sink. In that context, the absence of reported volcanic eruptions with VEI $\geq$ 5 since 1991 and low ENSO activity after 2000 facilitates this analysis.

Le Quéré et al. (2007) use ocean general circulation modelling plus inversion of southern atmospheric CO_2 data and find a slowing Southern Ocean CO_2 uptake of around 0.08 PgC yr^{-1} per decade, and this is supported in sign and magnitude by changes in South Indian Ocean fugacity measurements relative to the atmospheric change (Metzl, 2009). While the modelling results have been challenged (e.g. Boning et al., 2008; Law et al., 2008) and the fugacity measurements have large uncertainty and uneven temporal structure, even if correct, the magnitude of the flux changes is of marginal influence in the global context under discussion here. Also, the suggested sink decrease in the north Atlantic gyre (Watson et al., 2009) is in the wrong sense to help resolve the interhemispheric problem highlighted here. In terms

of magnitude, the post-2000 atmospheric growth attributable to reported emissions increases at 2.1 PgC yr^{-1} per decade, while our modelled global sinks increase at 0.9 PgC yr^{-1} per decade (approximately equally distributed between land and oceans).

More recently, Sarmiento et al. (2009) report an increase in the global terrestrial biosphere sink by 0.88 PgC yr^{-1} ($\sim$0.4 PgC yr^{-1} per decade) after 1988/1989 and decrease in global ocean sink by 0.35 PgC yr^{-1} ($\sim$0.2 PgC yr^{-1} per decade), reducing atmospheric accumulation by 0.53 PgC yr^{-1} over the same period ($\sim$0.3 PgC yr^{-1} per decade). Their conclusion about large increases in total land sink is based on similar emission estimates and NH atmospheric data (i.e. susceptible to misinterpretation of regional fluxes as being global) to those used by Le Quéré et al. (2009), but with partitioning between source/sink processes determined by the model based estimate of ocean sink. Bottom up estimates of land and ocean fluxes remain too uncertain to contribute to reliable estimates of global trends (e.g. their bottom-up estimate of total land sink change from 1988 to 1989 is equivalent to 1.1 ± 1.2 PgC yr^{-1}). Our measured atmospheric growth, adjusted for ENSO and volcanic influence, provides higher time-resolution than that described by Sarmiento et al., increasing at the historic rate of $\sim$0.5 PgC yr^{-1} per decade through the 1990s and slowing by $\sim$0.02 PgC yr^{-1} per decade after 2002/2003.

An accelerating terrestrial sink of the magnitude suggested by Sarmiento et al. (2009), constrained to be at mid-to-high northern latitudes by our suggested interhemispheric gradient constraint, raises serious concerns about the ability of the terrestrial sink to maintain such high rates into the future. However, there are other possible explanations of the atmospheric data.

6.3. *Anthropogenic emission estimates*

The Sarmiento et al. result is based on a 5% uncertainty in fossil fuel emissions which, while it may represent the present situation, significantly underestimates uncertainty in the 1990s (G. Marland and R. Andres, personal communication 2009). Recently, van Vuuren and Riahi (2008) have examined the quality of anthropogenic emissions inventory data, suggesting 'the recently observed increase in the rate of emission growth could very well turn out to be a statistical artefact', based primarily on uncertainties in Chinese emissions. Our suggested underestimation of 1990s emissions in order to reconcile modelled and observed growth from the 1990s is well within a 10–15% uncertainty of early emission estimates and offers a possible simple explanation for the surge in reported emissions, being a consequence of connecting systematic early underestimates (more subject to possible economic and/or political bias? or evolving methodology), with more accurate recent estimates.

7. Conclusions

The trend in global atmospheric CO_2 growth, thus in CO_2-induced global warming rate, is most reliably indicated in the large homogeneous CO_2 concentration fields in the troposphere south of 30°S. Annual accumulation of CO_2 in the atmosphere has marginally slowed after climate-induced high-northern-latitude peak emissions in 2002/2003, to fall below the four-decade baseline defined by a linear regression through Mauna Loa and South Pole growth-rate data (but still around $\sim$2 ppm yr^{-1} in 2009). Even if the global nature of our trends is contested, the ability of models to represent the precisely determined behaviour of such a large portion of the global troposphere is a strong and not-yet-adequately applied constraint on global budgeting models. A pressing requirement for abatement of anthropogenic climate forcing due to CO_2 is that the dC_a/dt approaches zero.

Adjustment for the historic (mainly equatorial) ENSO and volcanic influences (EV) on dC_a/dt suppresses large natural perturbations during the 1990s, achieving consistency with the four-decade linear growth trend. The EV correction is small and generally well correlated with CO_2 growth after 2002/2003, such that it does not contribute significantly to the 2003–2009 slowing in growth. A possible further slowing from 2008 may be indicative of reduced anthropogenic emissions associated with the Global Financial Crisis (Le Quéré et al., 2009), though uncertainty near the end of the smoothed records cannot yet exclude an ENSO-induced influence (but future better definition of the current ENSO cycle may do this).

The decadal behaviour contrasts with modelled atmospheric trends, dC_E/dt, attributable to fossil and land-use emissions using historically consistent C_a-dependent parametrizations of oceanic and terrestrial sinks. The dC_E/dt flatten through the 1990s and accelerate rapidly after 2000. Consistency with past dC_E/dt growth (due mainly to NH emissions) suggests there should be proportional increase in the interhemispheric CO_2 difference, which is not observed. In the absence of firm evidence for sufficiently large systematic bias in 1994–2003 terrestrial and/or oceanic sinks, systematic underestimation of emissions of around 6% is a simple and likely explanation for the dC_E/dt and dC_a/dt-EV trend differences. In this scenario, the recent responses of combined terrestrial and oceanic sinks to increasing atmospheric CO_2 remain broadly consistent with historic behaviour, and provide no evidence for volatility in the carbon cycle on a global scale. Alternatively, complex and unusual sink behaviour is required.

An approach that has been suggested for studying the recent dC_a/dt trend, is to seek statistical precedents for the observed trends. Although there have been periods in the past where dC_a/dt has decreased, a purely statistical approach such as this does not take into account available information on the causes for variations in the dC_a/dt. For example, dC_a/dt decreased around the early 1990s, but Pinatubo provides a likely explanation. The recent dC_a/dt decrease coincides with an unprecedented increase in reported anthropogenic forcing, and to date we have no independent information on natural sinks that would explain the observed decrease. Increasing global vigilance for anomalous

regional carbon fluxes limits possibilities for undetected natural contributions. Under these circumstances, measurements from continuous monitoring of selected mid-to-high latitude SH marine boundary-layer air offers readily accessible on-going strong constraints on global CO_2 emissions.

8. Acknowledgments

Valuable discussions on individual aspects of this work have been obtained from many CAWCR and international colleagues. In particular, Corinne Le Quéré, Gregg Marland and Skee Houghton have assisted with recent anthropogenic emission data, and reviewers plus Rachel Law have provided valuable advice on organization of the information. Ellsworth Dutton and Wlodek Zahorowski provided valuable data. The Australian Bureau of Meteorology Cape Grim Baseline Air Pollution Station and CSIRO GASLAB staff have provided excellence in the operation of developmental equipment and in collection of samples/data. For collection of samples at other flask sites we thank NOAA (USA), Meteorological Service of Canada, Australian Antarctic Division/Bureau of Meteorology and Australian Institute of Marine Science.

References

Allison, C. E. and Francey, R. J. 2007. Verifying Southern Hemisphere trends in atmospheric carbon dioxide stable isotopes. *J. Geophys. Res.* **112**, D21304, doi: 10.1029/2006JD007345.

Ashok, K., Behera, S. K., Rao, S. A., Weng, H. and Yamagata T. 2007. El Niño Modoki and its possible teleconnection. *J. Geophys. Res.* **112**, C11007, doi: 10.1029/2006JC003798.

Boning, C. W., Dispert, A., Visbeck, M., Rintoul, S. and Schwarzkopf, F. U. 2008. Antarctic circumpolar current response to recent climate change. *Nat. Geosci.* **1**, 864–869, doi: 10.1038/ngeo362.

Canadell, J. G., Le Quéré, C., Raupach, M. R., Field, C. B., Buitenhuis, E. T. and co-authors. 2007. Contributions to accelerating atmospheric CO_2 growth from economic activity, carbon intensity, and efficiency of natural sinks. *Proc. Natl. Acad. Sci. U.S.A.* **104**(47), 18866–18870.

Da Costa, G. A. and Steele, L. P. 1999. A low-flow analyser system for making measurements of atmospheric CO_2. In: *Report of the ninth WMO Meeting of Experts on Carbon Dioxide Concentration and Related Tracer Measurement Techniques* (eds R. J. Francey). Aspendale, Vic., (Environmental Pollution Monitoring and Research Programme/Global Atmosphere Watch 132; WMO/TD **952**). [Geneva]: Secretariat of the World Meteorological Organization. 16–20.

Denning, A. S., Rayner, P. J. Law, R. M. and Gurney, K. R. 2004. Atmospheric tracer transport model intercomparison project (Transcom) IGBP/GAIM Report Series, Report #4 (ed. Dork Sahagian), IGBP.

Dore, J. E., Lukas, R., Sadler, D. W., Church, M. J. and Karl, D. M. 2009. Physical and biogeochemical modulation of ocean acidification in the central north Pacific. *Proc. Natl. Acad. Sci. U.S.A.* **106**, 12235–12240.

Enting, I. G., Trudinger, C. M. and Etheridge, D. M. 2006. Propagating data uncertainty through smoothing spline fits. *Tellus* **B58**(4), 305–309.

Francey, R. J., Steele, L. P., Langenfelds, R. L., Lucarelli, M., Allison, C. E. and co-authors., 1996. Global Atmospheric Sampling Laboratory (GASLAB): supporting and extending the Cape Grim trace gas programs. In: *Baseline Atmospheric Program (Australia) 1993* (eds R. J. Francey, A. L. Dick and N. Derek). Bureau of Meteorology and CSIRO Division of Atmospheric Research, Melbourne, Australia, 8–29.

Francey, R. J. and Steele, L. P. 2003. Measuring atmospheric carbon dioxide—the calibration challenge. *Accredit. Qual. Assur. – J. Qual., Comparab. Reliab. Chem. Meas.* **8**(5) 200–204. doi: 10.1007/s00769-003-0620-1.

Gregg, J. S., Andres, R. J. and Marland G. 2008. China: Emissions pattern of the world leader in CO_2 emissions from fossil fuel consumption and cement production *Geophys. Res. Lett.* **35**(8), L08806.

Houghton, R. A. 2008. Carbon flux to the atmosphere from land-use changes: 1850–2005. In: *TRENDS: A Compendium of Data on Global Change*. Carbon Dioxide Information Analysis Center, Oak Ridge National Laboratory, U.S. Department of Energy, Oak Ridge, Tenn., USA.

Jones, C. D. and Cox, P. M. 2001. Modeling the volcanic signal in the atmospheric CO_2 record. *Global Biogeochem. Cycles* **15**, 453–465.

Keeling, C. D., Piper, S. C., Bacastow, M. Wahlen, R. B., Whorf, T. P. and co-authors. 2001. *Exchanges of Atmospheric CO_2 and $^{13}CO_2$ with the Terrestrial Biosphere and Oceans from 1978 to 2000. I. Global Aspects*, SIO Reference Series, No. 01–06, Scripps Institution of Oceanography, San Diego, 88 pp.

Keeling, C. D., Piper, S. C., Bacastow, R. B., Wahlen, M., Whorf, T. P. and co-authors. 2005. Atmospheric CO_2 and $^{13}CO_2$ exchange with the terrestrial biosphere and oceans from 1978 to 2000: observations and carbon cycle implications. In: *A History of Atmospheric CO_2 and its effects on Plants, Animals, and Ecosystems* (eds J. R. Ehleringer, T. E. Cerling and M. D. Dearing). Springer Verlag, New York, 83–113.

Langenfelds, R. L., Francey, R. J., Pak, B. C., Steele, L. P., Lloyd, J., and co-authors. 2002. Interannual growth rate variations of atmospheric CO_2 and its isotope $\delta^{13}C$, H_2, CH_4 and CO between 1992 and 1999 linked to biomass burning. *Global Biogeochem. Cycles* **16**, 1048, doi: 10.1029/20001GB001466 (2002).

Law, R. M., Matear, R. J. and Francey, R. J. 2008. Comment on "Saturation of the Southern Ocean CO_2 sink due to recent climate change". *Science* **319**(5863), 570a. doi: 10.1126/science.1149077.

Le Quéré, C., Rödenbeck, C., Buitenhuis, E. T., Conway, T. J., Langenfelds, R. L. and co-authors. 2007. Saturation of the Southern Ocean CO_2 sink due to recent climate change. *Science*, doi: 10.1126/science.1136188.

Le Quéré, C., Raupach, M. R., Canadell, J. G., Marland, G., Bopp, L. and co-authors., 2009. Trends in the sources and sinks of carbon dioxide. *Nat. Geosci.* **2**, Focus/Progess Article, December 2009, doi:10.1038/NGEO689.

Marland, G., T. A. Boden and R. J. Andres. 2008. Global, regional and national CO_2 emissions. In *Trends: A Compendium of Data on Global Change*. Carbon Dioxide Information Center, Oak Ridge National Laboratory, U. S. Department of Energy, Oak Ridge, Tenn., USA.

Masarie, K. A., Langenfelds, R. L., Allison, C. E., Conway, T. J., Dlugokencky, E. J. and co-authors. 2001. NOAA/CSIRO Flask Air Intercomparison Experiment: a strategy for directly assessing consistency among atmospheric measurements made by independent laboratories. *J. Geophys. Res.* **106**(D17) 20445–20464.

Metzl, N. 2009. Decadal increase of oceanic carbon dioxide in Southern Indian Ocean surface waters (1991–2007) *Deep-Sea Res. II* **56**, 607–619.

Miyazaki, K., Patra, P. K., Takigawa, M., Iwasaki, T. and Nakazawa. 2008. T. Global-scale transport of carbon dioxide inthe troposphere. *J. Geophys. Res.* **113**, D15301, doi: 10.1029/2007JD009557.

Page S. E., Seigert, F., O Rieley, J., Boehm H-D. V., Jaya, A., and co-authors. 2002. The amount of carbon released from peat and forest fires in Indonesia during 1997. *Nature* **420**, 61–65. doi: 10.1038/nature01131.

Randerson, J. T., Van Der Werf, G. R., Collatz, G. J., Giglio, L., Still, C. J. and co-authors. 2005. Fire emissions from C3 and C4 vegetation and their influence on interannual variability of atmospheric CO_2 and $\delta^{13}CO_2$. *Global Biogeochem. Cycles*, **19**, GB2019, doi: 10.1029/2004GB002366.

Randerson, J. T., Van Der Werf, G. R., Tosca, M., Kai, F.-M., Chen, Y. and co-authors. 2009. Climate-fire feedbacks in tropical ecosystems: Insight from a 12-year satellite time series of global fires. ICDC8 Extended Abstract.

Raupach, M., Canadell, J. and Le Quere, C. 2008. Anthropogenic and biophysical contributors to increasing atmospheric CO_2 growth rate and airborne fraction. *Biogeosciences* http://www.biogeosciences-discuss.net/**5/**2867/2008/bgd-5-2867-2008.pdf.

Raupach, M. R., Marland, G., Ciais, P., Le Quéré, C., Canadell, J. G. and co-authors. 2007. Global and regional drivers of accelerating CO_2 emissions. *Proc. Natl. Acad. Sci. U.S.A.* doi: 10.1073/pnas.0700609104.

Rayner, P. J., Law, R. M., Allison, C. E., Francey, R. J., Trudinger, C. M. and co-authors. 2008. The interannual variability of the global carbon cycle (1992–2005) inferred by inversion of atmospheric CO_2 and $^{13}CO_2$ measurements. *Global Biogeochem. Cycles* **22**, doi: 10.1029/GBC2007GB003068.

Reichstein, M., Ciais, P., Jung, M., Beer, C., Bahn, M., Carvalhais, N. and co-authors. 2009. The role of climate variability and extremes for global terrestrial carbon dynamics: lessons learnt from multiple observations and experiments. In *Climate Change: Global Risks, Challenges and Decisions* IOP Publishing, IOP Conf. Series: Earth and Environmental Science 6 042006 doi: 10.1088/1755-1307/6/4/042006.

Sarmiento, J. L., Gloor, M., Gruber, N., Beaulieu, C., Jacobson, A. R. and co-authors. 2009. Trends and regional distributions of land and ocean carbon sinks. *Biogeosci. Discuss* **6**, 10583–10624, www.biogeosciences-discuss.net/6/10583/2009/

Stephens, B. B., Gurney, K. R., Tans, P. P., Sweeney, C., Peters, W. and co-authors. 2007. The vertical distribution of atmospheric CO_2 defines the latitudinal partitioning of global carbon fluxes. *Science* **316**, 1732–1735.

Thoning, K. W., Tans, P. P. and Komher, W. D. 1989 Atmospheric carbon dioxide at Mauna Loa observatory, 2. Analysis of the NOAA/GMCC data, 1974–1985. *J. Geophys. Res.* **94**, 8549–8565.

Trudinger, C. M., Enting, I. G., Francey, R. J. and Etheridge, D. M. 1999. Long term variability in the global carbon cycle inferred from a high precision CO_2 and $\delta^{13}C$ ice core record. *Tellus* **51B**, 233–248.

Van Vuuren, D. P. and Riahi, K. 2008. Do recent emission trends imply higher emissions forever?. *Clim. Change* **91**, 237–248. doi: 10.1007/s10584-008-9485-y.

Vetter, M., Churkina, G., Jung, M., Reichstein, M., Zaehle, S. and co-authors. 2008. Analyzing the causes and spatial pattern of the European 2003 carbon flux anomaly using seven models. *Biogeosciences* **5**, 561–583. www.biogeosciences.net/5/561/2008/.

Watson, A. J., Schuster, U., Bakker, D. C. E., Bates, N. R., Corbière, A. and co-authors. 2009. Tracking the variable North Atlantic Sink for atmospheric CO_2, Science **4**, 1391–1393, doi: 10.1126/science.1177394

WMO. 2008. WDCGG No. 32, GAW Data Volume IV- Greenhouse Gases and Other Atmospheric Gases. Japan Meteorological Agency in cooperation with World Meterological Organization.

Zahorowski, W., Chambers, S., Wang, T., Kang, C-H., Uno, I. and co-authors. 2005. Radon-222 in boundary layer and free tropospheric continental outflow events at three ACE-Asia sites. *Tellus* **57B**, 124–140.

Supporting Information

Additional supporting information may be found in the online version of this article.

Appendix S1: Selection of marine boundary layer air at Cape Grim.

Appendix S2: Growth rate error from measurement bias.

Appendix S3: ENSO and volcanic influence on CO_2 growth rate.

Appendix S4: Modelled response to emission estimates.

Please note:Wiley-Blackwell are not responsible for the content or functionality of any supporting materials supplied by the authors. Any queries (other than missing material) should be directed to the corresponding author for the article.